Parametric Experimental Study of Ultra-Short Stud Connections for Lightweight Steel–UHPC Composite Bridges

Qizhi Xu[1], Wendel Sebastian[2], Kaiwei Lu[3], Yiming Yao[4], Jingquan Wang[5*]

Abstract

This paper reports on double shear push-out tests conducted on steel-to-ultra-high performance concrete (UHPC) connections based on studs of 30 mm or 22 mm diameter in slabs of 35, 55 or 150 mm thickness. The results show that with increase in stud diameter, the longitudinal shear strength improved by 25% and 94% for ultra-short and long studs (of aspect ratios below and equal to 4.0) respectively. For short studs both the aspect ratio and concrete cover greatly influenced failure by partial stud fracture or UHPC pryout, while the diameter governed failure behaviour for long studs. Decreases in aspect ratio and cover thickness caused shear resistance to drop by 40% and 7% respectively for 30 and 22 mm diameter studs. Regression analyses show that the shear strength, slip stiffness and ductility of the connections are exponential, sinusoidal and polynomial functions respectively of the stud aspect ratio. The ultra-short stud-UHPC connections are 62% stiffer in slip than their normal concrete counterparts. Future work should entail fatigue testing of the connections.

Keywords: Ultra-short stud; Ultra-high Performance Concrete (UHPC); Load-slip; Composite structures; Shear connection

[1]PhD student, Civil Engineering Dept, Southeast University, Nanjing 210096, China; Currently Visiting PhD student, CEGE Dept, University College London, London WC1E 6BT, UK. E-mail: qizhixu@seu.edu.cn
[2]Reader, Civil, Environmental and Geomatic Engineering (CEGE) Department, University College London, Chadwick Building, Gower Street, London WC1E 6BT, UK. E-mail: W.Sebastian@ucl.ac.uk
[3]PhD student, Civil Engineering Dept, Southeast University, Nanjing 210096, China. E-mail: lkw@seu.edu.cn
[4]Associate professor, Civil Engineering Dept, Southeast University, Nanjing 210096, China. E-mail: yiming.yao@seu.edu.cn
[5]Professor, Department of Civil Engineering, Southeast University, Nanjing 210096, China. (Corresponding author) E-mail: wangjingquan@seu.edu.cn

Introduction

Steel–concrete composite bridges are widely used for their convenient construction and attractive mechanical behavior (Lin et al. 2016; Mosallam et al. 2014; Su et al. 2014; Xue et al. 2012). If the deck uses normal concrete (NC), then live load negative moments on the composite section induce cracks, which may lead to rebar corrosion, less bond and lower stiffness (Wang et al. 2019a; Zhao et al. 2018; Hamoda et al. 2017; Lin et al. 2014; Yoshitake et al. 2016), which are exacerbated by the harsher environments around bridges.

Replacing NC with ultra-high performance concrete (UHPC) shows promise (Hamoda et al. 2017; Hossain et al. 2016; Liu et al. 2019b; Zhang et al. 2017a). UHPC comprises cement, fine aggregates, steel fibers and superplasticizer (Shafieifar et al. 2018). Relative to NC it possesses higher compressive (> 150 MPa) and tensile (> 7 MPa) strengths, as well as superior post-cracking behavior due to the dispersed steel fibers. Thus, it has the potential to enable thin and durable deck systems so that self-weight can be significantly reduced and the service life remarkably extended (Naaman and Chandrangsu 2004; Russell and Graybeal 2013; Yang et al. 2011). These features of UHPC can accelerate the development and use of lightweight steel–concrete composite bridges with excellent mechanical performance (Liu et al. 2019c; Luo et al. 2019; Shao et al. 2018; Zhang et al. 2017a).

Shao et al. (2013) and Cao et al. (2016) proposed a composite system comprising a conventional orthotropic steel deck (OSD) with a UHPC layer to avoid fatigue damage. Analysis and field monitoring of the Fochen West and Haihe bridges showed significantly reduced vehicle-induced stress ranges and effectively enhanced fatigue resistance by using a

50 mm thick UHPC layer (Shao et al. 2018; Zhu et al. 2018). Yoo and Choo (2016) proposed an inverted T-steel beam to optimise composite action by removing the beam flange, and welding the studs in horizontal layout to both sides of the web. Longitudinal cracks in the UHPC slab were generated in this system with large stud spacing, with ductile behavior observed in positive flexure. Wang et al. (2019b) studied the performance of steel–UHPC composite beams with different interfacial treatments under positive bending, where 60 mm thick UHPC slabs were used. The test results showed that an epoxy adhesive with sprinkled limestone aggregate could replace the stud connector under certain conditions.

Alongside the UHPC, shear stud connections also play a key role in improving structural action. Studs embedded in thin steel fiber-reinforced concrete slabs have attracted much research attention (Cao et al. 2017; Kim et al. 2015; Liu et al. 2019c; Luo et al. 2016b). The studies indicate that a thinner bridge deck could be constructed with UHPC instead of NC because of its improved compressive strength and crack resistance. Thinner slabs allow use of short studs with low aspect ratios (defined as the ratio of the stud's height to its shank diameter). However, in NC–steel composite structures, a stud aspect ratio of 3.26 is suggested for failure of both concrete and steel materials (Ollgaard et al. 1971). An aspect ratio higher than 4.5 is only for shank failure (Precast/Prestressed Concrete Institute (PCI) 2004). If the aspect ratio is increased from 4.5 to 5.5, the possibility of shank failure increases from 81.6% to 84.5% (Pallarés and Hajjar 2010). A minimum aspect ratio of 3.0 is specified by Eurocode 4 (2 CEN 2005) and 4.0 by American Association of State Highway Officials (AASHO) and Load-and-Resistance Factor Design (LRFD) (AASHTO 2020).

Studies on short studs employed in steel–UHPC connections have been conducted.

Kim et al. (2015) revealed that the stud aspect ratio could be reduced from 4 to 3.1 without loss of shear strength. From push-out tests, Cao et al. (2017) suggested a minimum aspect ratio of 2.7 when stud fracture is dominant. Luo et al. (2016a; b) also studied the behavior of grouped studs with an aspect ratio of 3.6 via push-out tests. The results indicated that stud fracture could be ensured even without any rebar because of the high tensile strength of UHPC. Wang et al. (2017) proposed a demountable headed stud connector, which was screwed at the headed stud and connected through a pre-punched hole to a steel beam by nuts. Aspect ratios varying from 1.05 to 3.16 were investigated. Stud fracture without cracks on the slabs was observed for studs with aspect ratios exceeding 1.5. However, tensile failure due to UHPC pryout occurred with a further decrease in the aspect ratio.

These findings highlight the potential of short studs in thin UHPC slabs. In order to ensure their successful use in lightweight steel–UHPC composite bridges, the performance of such studs must be studied for a range of slab depths, stud diameters and aspect ratios.

To those ends, in the present study, 22 mm and 30 mm (large) diameter studs were used as connectors in 21 push-out steel–UHPC test specimens. Based on the tests the influences of stud diameter, stud aspect ratio and UHPC cover thickness are analysed, while the failure modes, shear bearing capacity and interfacial slip behavior are evaluated. Regression analyses of the data are used to express connection shear capacity, slip stiffness and ductility as functions of stud' aspect ratio. The performance of these connections is compared to that of traditional studs in NC. In closing, the need to study fatigue performance is highlighted.

Experimental program

Specimen details and material properties

Table 1 and Fig. 1 show that each double-shear specimen used a HW250 × 255 × 14 × 9 (GB50017-2003) hot-rolled steel beam (diagram and dimension shown in Fig. 1) with eight welded studs. The seven sets of three repeated specimens cover three slab thicknesses (150, 55, 35 mm), two stud diameters (22, 30 mm) and three stud heights (120, 45, 30 mm) to give five stud aspect ratios (4, 2, 1.5, 1.4, 1), and with five cover concrete thicknesses (120, 105, 30, 10, 5 mm) above the studs. To ensure that the steel beam was not embedded in the concrete slab, the steel beam and the lateral formwork of the concrete slab were fixed by a wooden brace to restrict deformation during casting and curing of the concrete.

Longitudinal and transverse steel reinforcing deformed bars of grade HRB400 (GB 50010-2010) of diameters 10 mm and 8 mm (photos shown in Fig. 1), respectively, were placed in the UHPC slab, whose nominal yielding stress was 400 MPa, but were tested 504 MPa and 418 MPa for 10 mm and 8 mm diameter bars, respectively. The transverse reinforcement ratio was kept constant. Two layers of rebar with hoops were placed in the 150 mm thick UHPC slab, while only one layer of reinforcement was placed in the thinner slabs.

Table 1 Details of the push-out specimens

Specimen group	Deck thickness （mm）	Stud shear connector			Cover thickness (mm)	Number of Replicates
		Diameter (mm)	Height (mm)	Aspect ratio (Height/diameter)		
D22T150-I	150	22	30	1.4	120	3
D22T150-II	150	22	45	2.0	105	3
D30T150	150	30	120	4.0	30	3
D22T55	55	22	45	2.0	10	3
D30T55	55	30	45	1.5	10	3

D22T35	35	22	30	1.4	5	3
D30T35	35	30	30	1.0	5	3

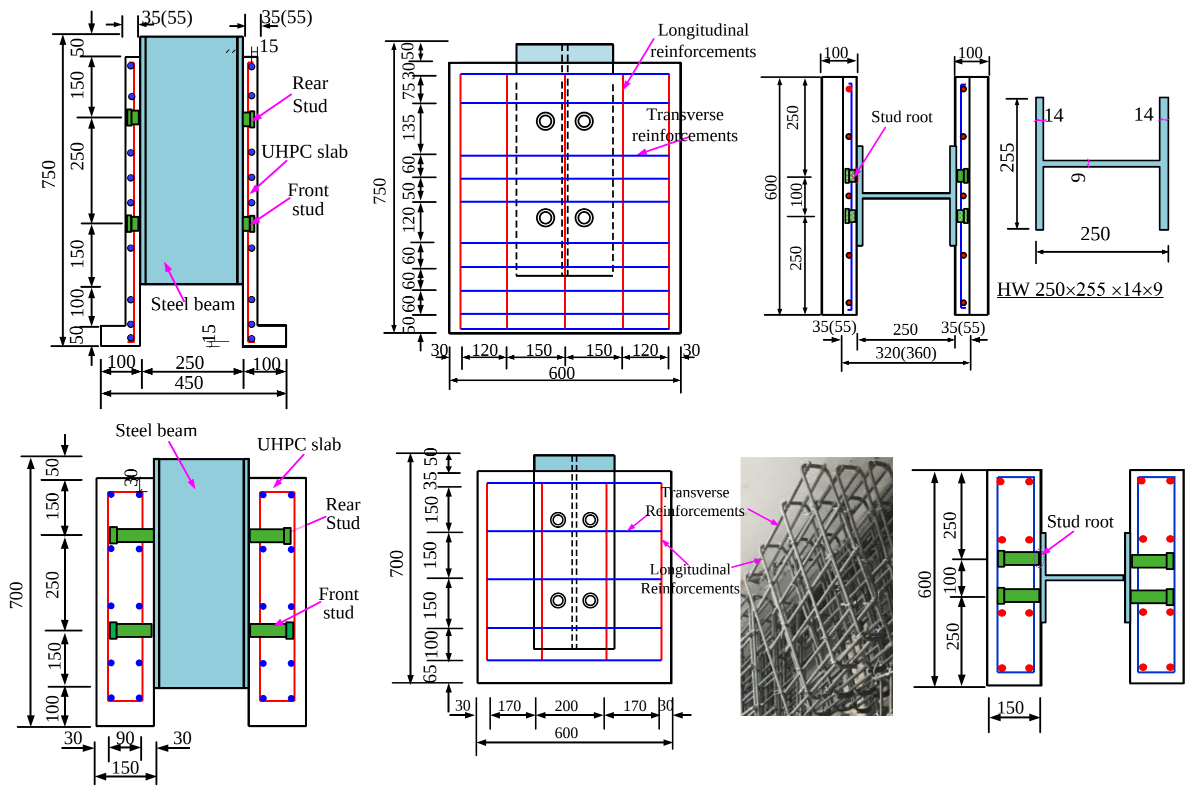

(a) Front view (b) Side view (c) Top view

Fig. 1 Details of specimens (Unit mm)

The UHPC composition is presented in Table 2. The water-to-cementitious materials ratio of the UHPC (W/B) in this study was 0.15. The cementitious materials were mainly composed of cement (P II 52.5 cement), silica fume (particles smaller than 1 mm, surface area of 20,000 m^2/kg, SiO_2 content of 95%) and medium coarse sand (5 mm maximum particle size and 2.6 fineness modulus). Steel fibers (0.2 mm in diameter and 13 mm in length) and a special active admixture SBT®-PCA (Wang et al. 2018), developed by Subote Materials Co. Ltd, were added. Additionally, fly ash in the form of microsphere (micro-bead) and superfine mineral powder were added into the UHPC to further reduce the cement and silica fume, thus reducing cost and environmental impact (Meng and Khayat 2016).

Table 2 Components and properties of the UHPC

Component	Weight (kg/m^3)	Mechanical properties (MPa)		
Cement	939.2	Cube compressive strength	Average	125
Silica fume	58.7		Standard deviation	2.5
Micro-bead	93.92	Prism Compressive strength	Average	130
Superfine mineral powder	82.18		Standard deviation	1.9
Sand	933	Tensile strength	Average	7.2
High active admixture	28		Standard deviation	0.3
Steel fiber	160	Elastic modulus	Average	46500
Water	175		Standard deviation	600
Water–binder ratio (W/B)	0.15			

Note: The steel fiber used in the UHPC was straight steel fiber with D = 0.2 mm and L = 13 mm, where D denotes the fiber diameter and L the fiber length.

To obtain the compressive strength, three 100 mm cubes and three 100 × 100 × 300 mm prism blocks were tested to standard GB/T 31387-2015, while three 50 × 500 × 100 mm dog-bone samples were prepared to measure the direct tensile strength consistent with the method used by Liu et al. (2019a). The UHPC specimens were cured at standard room temperature for 28 days. The average and standard deviation value for compressive strengths, shown in Table 2, were 125 ± 2.5 MPa and 130 ± 1.9 MPa for three cube and prism specimens, respectively, while the initial elastic modulus and tensile strength were 46.5 ± 0.6 GPa and 7.2 ± 0.3 MPa, respectively.

The studs, due to their size and geometry, custom coupons were fabricated by removing the head of the stud to match well with the anchorage end of the experimental machine (Kruszewski et al. 2018). The stud shank of 500 mm length and the rebars of 1.5 m length were tested in uniaxial tension until fracture, and thereby the obtained strength. The 30 mm diameter studs were of yield and ultimate stresses 468 MPa and 525 MPa, respectively, as obtained from tension tests. The corresponding measured strengths of the 22 mm studs were 412 MPa and 480 MPa, respectively.

Test setup and instruments

Fig. 2 illustrates the test setup and details of the push-out specimens, which are labeled according to the stud diameter and UHPC slab thickness. For example, D30T150 refers to 30 mm diameter studs embedded in a 150 mm thick UHPC slab. Load was applied using a 5000 kN YAS-5000 compression testing machine (accuracy of 0.01 kN). The specimens were placed on a steel platform, and the load was applied through the spreading steel plate on top of the steel beam. To ensure uniform contact of the UHPC with the machine base, a layer of sand was placed under the slab. The average slip was obtained from the four dial gauges located on the sides. Two dial gauges (maximum 12.7 mm in range and 0.01 mm in accuracy) were attached to the steel beam to measure transverse uplift. The crack widths were inspected by a visual crack observation device, whose accuracy was 0.01 mm. Trial loading-unloading cycles were manually performed prior to the shear test to ensure functionality of the loading system. Subsequently, the actual tests were conducted via manual loading with load increments of 40-50 kN until the load-displacement visually softened, after which, the load increments were decreased to 20 kN for the remainder of the testing. Load and slip values were recorded at the end of each load increment.

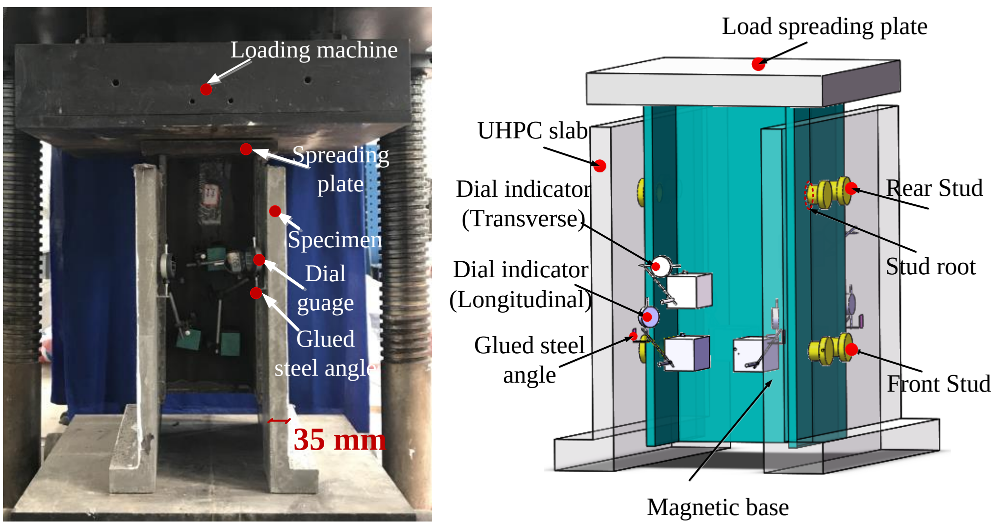

(a) Layout of specimen (b) View of measuring points

Fig. 2 Static test setup and measuring point arrangement

Results and discussion

Failure modes

Three failure modes, namely complete or partial fracture of the studs, or UHPC pryout, were noted. Images of the failure modes and crack distributions are shown in Figs. 3 and 4.

Fig. 3 Typical failure modes of specimens

It was observed that all studs embedded in the 150 mm UHPC slab fractured, as displayed in Figs. 3 (a)–(d). Only small voids behind the stud and minor local crushing of UHPC under the stud root (where it was welded to the beam) were observed. The 22 mm diameter studs fractured for aspect ratios in the range 2.0 - 1.4. However, different failure modes were observed for the 30 mm diameter studs, as the stud aspect ratio decreased from 4.0 (D30T150) to 1.5 (D30T55) and 1.0 (D30T35). In the D30T55 group, both stud complete fracture accompanied by local crushing of the UHPC (Figs. 3 (e, f)) and partial fracture characterized by stud fracture mixed with stud pullout (Figs. 3 (g–j)), all at the base of the shank, were observed. A higher stud diameter (and hence stiffness) in the thin UHPC slab might have caused variations in the failure modes and uneven redistribution of loads between studs. Pryout failure of the UHPC and complete pullout of studs dominated as the slab thickness reduced to 35 mm, where the stud aspect ratio was 1.0, see Figs. 3 (k, l).

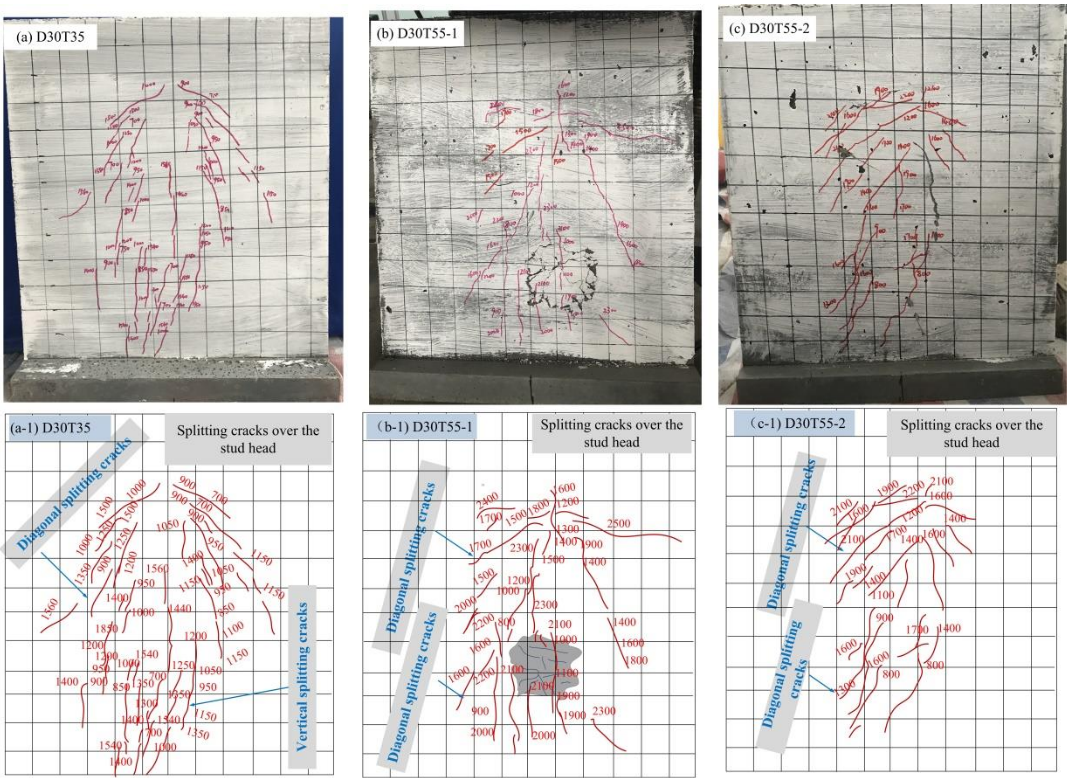

Fig. 4 Crack distributions on external slab surfaces

Figs. 4(a-c) show some diagonal splitting cracks around the studs on the thin slab surfaces of specimens D30T35 and D30T55, in which the numbers near the red lines (which define the cracks) denote the loads at which the cracks were first observed. By contrast, no cracks were observed in specimens D22T150 and D30T150. For the 55 mm thick UHPC slab with a 1.5 stud aspect ratio (Figs. 4 (b-c, b-1, c-1)), diagonal and vertical splitting cracks were noted. Dense diagonal cracks were distributed over a wide region around the rear studs, and vertical splitting cracks initiated near the front studs for specimen D30T35 (Fig. 4 (a, a-1)). The maximum crack widths at failure were observed for the 35 mm and 55 mm thick slab specimens, for which the average values were 0.13 mm (D22T35), 0.18 mm (D22T35), 0.15 mm (D22T55), and 0.43 mm (D30T55), respectively.

Ultimate shear strength and interfacial behavior

The test results are displayed in Table 3, where $\overline{P_{max}}$ is the average load borne by each stud and δ_u is the average slip at peak load. Also, SF, SPF/UP and UP refer to stud fracture, stud partial fracture with UHPC pryout and UHPC pryout failure, respectively. The Table shows that the average capacities of specimens with stud diameters of 22 mm seem almost independent of the slab thickness and stud height, although the average capacity of specimens D22T35 is 8% lower.

Table 3 Summary of test results

Group	$\overline{P_{max}}$ (kN)	$\overline{S_{max}}$ (mm)	CoV (P_{max})	Avg (Ks)	CoV (Ks)	Avg (μ_s)	CoV (μ_s)	Failure mode
D22T150-I	190.2	3.02	0.03	542.0	0.12	1.44	0.25	SF
D22T150-II	194.8	2.39	0.16	450.7	0.37	2.23	0.30	SF
D30T150	377.3	5.59	0.01	648.2	0.23	3.44	0.48	SF
D22T55	190.3	4.97	0.14	498.2	0.16	3.85	0.25	SF
D30T55	304.2	3.34	0.07	625.1	0.02	2.27	0.09	SF、SPF/UP
D22T35	178.6	2.62	0.02	568.2	0.07	1.44	0.25	SF
D30T35	226.3	1.22	0.11	547.0	0.04	0.63	0.31	UP

Note: $\overline{S_{max}}$ indicates the average maximum slip amount corresponding to the average peak load $\overline{P_{max}}$. Avg refers to the average value in each group. CoV denotes the coefficient of variation. K_s is the initial shear stiffness, μ_s refers to the ductility. SF, SPF/UP and UP denote the stud fracture failure, stud partial fracture/UHPC pryout, and UHPC pryout failure, respectively.

Figs. 3 and 4 show that for large studs, the varying cover thickness and stud aspect ratio caused different stud-UHPC interaction mechanisms and failure modes. Fig. 5

(presenting normalized load–slip plots) shows that the connections represented on the plot exhibited ductile behavior over slip ranges between 50% and 70% of the ultimate slip capacity.

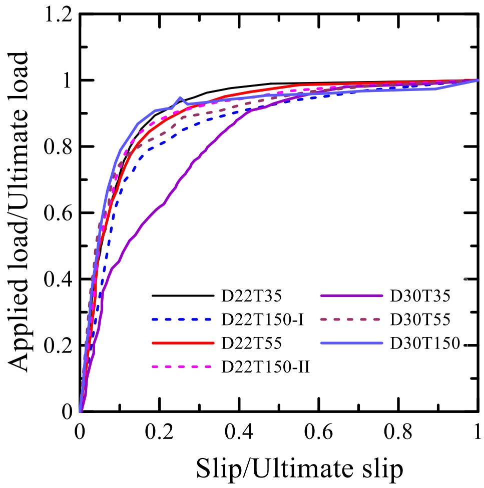

Fig. 5 Normalized load–slip relationship

Effects of stud diameter

For the 35 mm thick UHPC slab, Fig. 6 (a) shows that the average ultimate shear strength improved by 26.7% and the interfacial slip dropped by 53% as the stud diameter rose from 22 to 30 mm. The failure mode shifted from stud complete fracture to UHPC pryout due to insufficient stud anchor capacity in the UHPC slab to resist the increased local bending and tension (Wang et al. 2017). A higher strength was expected due to the larger stud diameter. A marginal portion of the UHPC was crushed under each stud root, but some portions were torn off and attached to the pulled-out stud (Figs. 3 (k, l)). The exceptional tensile properties of the UHPC were expected to be better utilized for specimen D30T35 where more splitting was observed. Fig. 6(a) also shows that slip beyond the yield point of specimen D30T35 is smaller than that of D22T35, implying that UHPC pryout due to stud flexing inhibited further slip before failure.

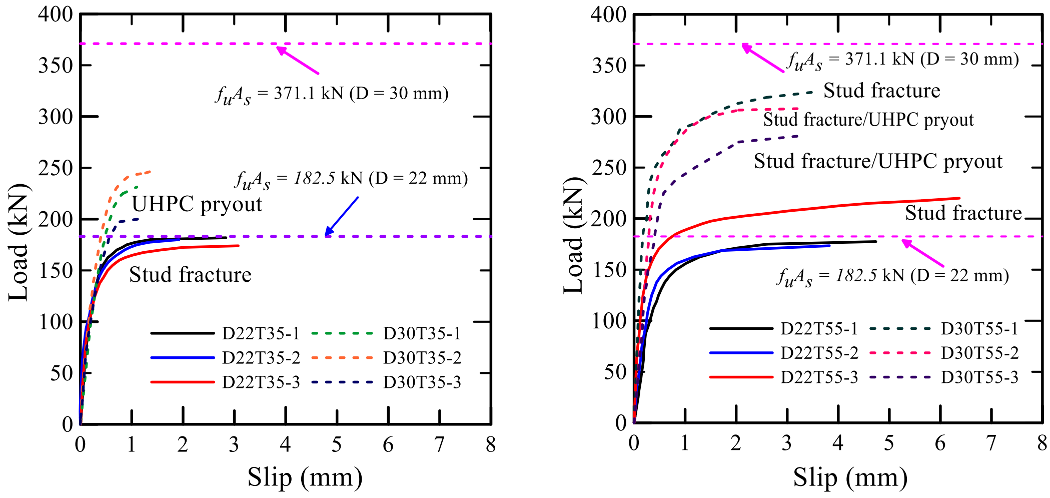

(a) Slab thickness = 35 mm (b) Slab thickness = 55 mm

Fig. 6 Effects of stud diameter (per stud)

For specimens of 55 mm slab thickness, an 85% increased cross-sectional area of the stud (i.e., from 22 to 30 mm diameter) led to a 60% increase of the average ultimate shear strength. The studs in specimen D30T55-I showed remarkable flexure at failure, leading to severe UHPC failure. For specimens D30T55-II and D30T55-III, the inclined fracture surface of the stud was observed with some attached UHPC, suggesting pronounced flexure–shear deformation. Hence, specimen D30T55-I had 6% and 15% higher ultimate shear strength than D30T55-II and D30T55-III, respectively. Lower strength for large-diameter stud connections was obtained due to UHPC pryout failure (Wang et al. 2017) as the UHPC slab thickness was decreased in the current study. Specimen D30T55 exhibited a more pronounced failure portion of the UHPC around the stud compared to D22T55 (Fig. 3), leading to a smaller bonding force and more flexure of the stud (Okada et al. 2006). The different failure modes illustrated that this local flexure and the UHPC pryout behavior led to smaller increases in shear resistance than the increases in stud cross-sectional area.

For the 150 mm thick UHPC slab, it is seen from Table 3 that the shear strength varies with the stud's cross-sectional area, owing to the stud fracture failure mode. Since only crushing of the UHPC occurred local to the root of the stud with no visible cracks, the failure modes were mainly affected by the shear–compression zone under the stud root. Moreover, the slip capacity of specimen D30T150 exceeded that of specimen D22T150 due to the larger crushing UHPC portion and higher loads prompted by the larger diameter studs.

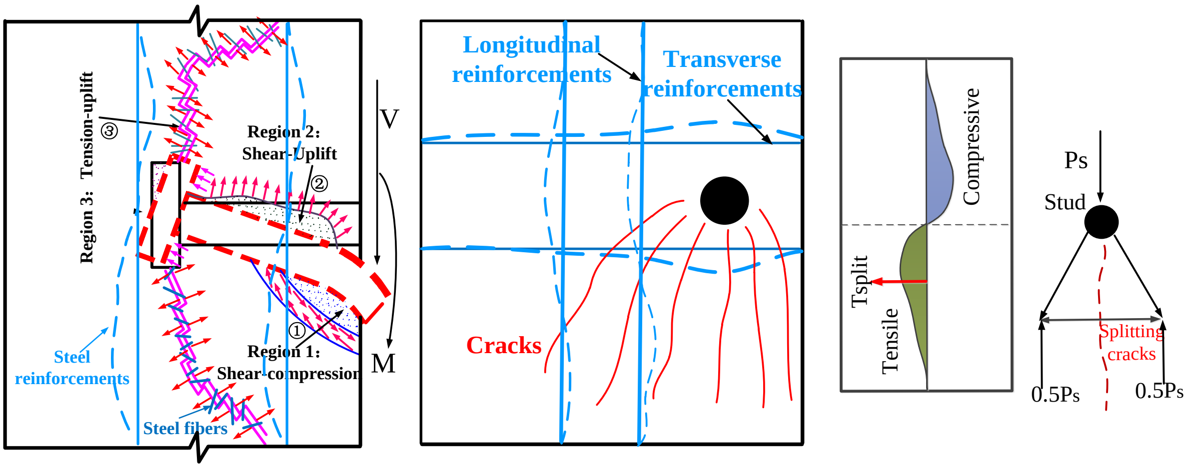

(a) Stud-UHPC interaction (b) Splitting cracks (c) Splitting mechanisms

Fig. 7 Schematic of mechanisms of stud–UHPC interaction

Fig. 7 depicts three major influence regions of the stud–UHPC interactions based on the failure modes and crack distributions (Fig. 7(a)), namely the shear–compression region under the root of the stud, the shear-uplift region along the shank, and the tension-uplift region at the head of the stud. The arrows in the figures indicate the stresses which acted on the UHPC and the stud to have triggered failure. The tension vectors with an inclined plane across the boundary around the stud head indicated a cone failure of UHPC. The red line in Fig. 7(b) denotes where the splitting cracks occurred whereas the solid and dashed blue lines represent the undeformed and deformed rebars, respectively. Fig. 7(c) shows the splitting mechanisms, the stress distribution in UHPC and the red arrows indicated the resultant force (T_{spit}). The local steel rebars helped control the evolution of cracks and occurrence of splitting as illustrated in Figs. 7(b-c). Note that the transverse rebars helped resist longitudinal splitting and retarded crack propagation, while the longitudinal rebars helped restrain expansion of concrete around the stud. Table 4 shows the influence on the interfacial shear resistance of these active regions for different stud diameters.

Table 4 Major influence regions for different stud diameters

Slab thickness (mm)	Diameter (mm)	Height (mm)	Major influence regions
35	22	30	①③
	30	30	①②③
55	22	45	①③
	30	45	①②③
150	22	30	①
	22	45	①
	30	120	①

The shear-compression region was associated with the stud shear fracturing due to the shear deformation. The shear-uplift region indicated that the shear deformation of stud and UHPC pryout behavior produced the pronounced influence on the shear strength. In the tension-uplift region, the UHPC cover over the stud head induced an anchorage problem at the stud head, and led to the occurrence of stud flexure deformation and splitting cracks. Therefore, shear–compression and tension-uplift regions were in control of the failure for specimen D22T35 (which failed by stud fracturing and numerous cracks of UHPC slab) while regions of shear-uplift and tension-uplift more significantly affected the failure of specimen D30T35 (which failed by stud pullout with UHPC pryout and numerous splitting cracks). Additionally, the regions of tension-uplift, shear-uplift, and shear–compression had significant influences on the interfacial shear behavior for specimen D30T55 (which failed by stud fracture, UHPC pryout and numerous splitting cracks), whereas specimen D22T55 was mainly affected by the tension-uplift and shear–compression regions because of marginal stud flexure deformation. The specimen comprising a 150 mm thick slab was primarily affected by shear-compression region because of stud fracturing.

Effects of slab thickness and UHPC cover thickness

Fig. 8 presents the load–slip relationships for varying cover and slab thicknesses. Table 3 and Figs. 8(a-b) show that only 8% variation of the shear strength for the 22 mm stud in UHPC slabs was observed as the slab thickness dropped from 150 to 55 and 35 mm. This suggests that slab thickness negligibly influenced shear strength while failure occurred by stud fracture. However, the stud was shortened for compatibility with a thinner slab, which might make the failure mode shift from complete stud fracture to UHPC pryout (Figs. 3 (e–l)). Fig. 8 (c) shows that the shear strengths of the large-diameter stud specimens decreased by 25% and 42%, respectively, accompanied by the decreased ultimate slip capacity as the slab thickness decreased from 150 to 55 and 35 mm. This showed that ultra-short studs in thin UHPC slabs led to the different stud-UHPC interaction mechanisms.

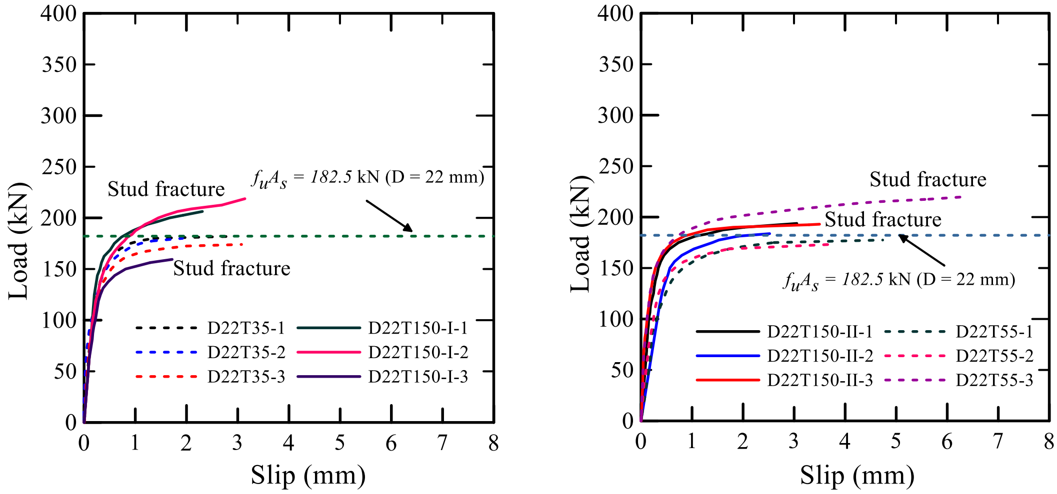

(a) Thickness = 35/150 mm (b) Thickness = 55/150 mm

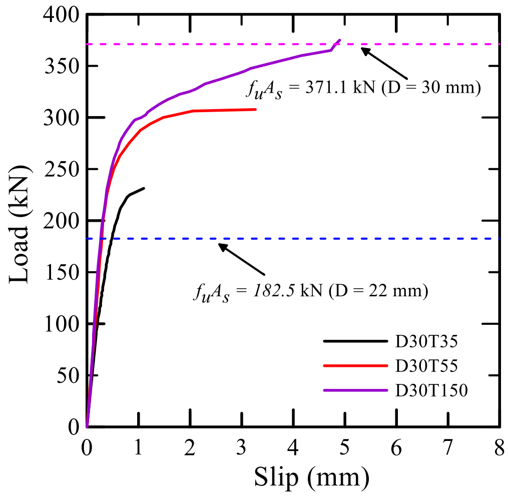

(c) Thickness = 35/55/150 mm

Fig. 8 Effects of cover thickness

Fig. 9 depicts three stud–UHPC interactions corresponding to the experimental findings for different studs and slab thicknesses, where the arrows referred to the same meaning as shown in Fig.7. Fig. 9 (a) illustrates the shear-compression region (studs embedded in the 150 mm UHPC slab) and Fig. 9 (b) displays the flexure–shear deformation of the stud in a thinner (55 mm thick) UHPC slab. Owing to the small cover thickness, the tension-uplift region above the stud head might become larger to provide sufficient resistance and thus the shear–compression and shear-uplift regions significantly affected the failure mode. Fig. 9 (c) illustrates that the three regions overlapped as the slab thickness dropped further to 35 mm. Flexure then prevailed, and a wider tension-uplift zone extended the crack to the slab surface, thus reducing confinement of the stud head.

Additionally, cover thickness had a great influence on the crack distribution on the external slab surface, and thus affected the stud failure. A UHPC cover thickness of 30 mm was sufficient to resist the splitting cracks, which is lower than the value of 50 mm stipulated in the AASHTO (AASHTO 2020) for normal concrete. As the cover thickness was reduced to 15 and 5 mm, numerous flexural cracks at the stud head and splitting cracks under the stud root initiated and developed at lower applied loads (see Fig. 4), resulting in smaller restrictions to the stud head and larger stud bending deformation (Okada et al. 2006). Therefore, the compressive stress parallel to the shank from the surrounding UHPC was impaired, and thus, the triaxial stress under the shear–compression region was weakened. Then, the pryout force in the stud accordingly increased owing to a larger transverse expansion of concrete and larger bending deformation of stud (Pavlović et al. 2013). Consequently, stud pullout gradually governed because of insufficient anchorage capacity. Hence, the interfacial shear strength and slip capacity were reduced with a decrease in cover thickness.

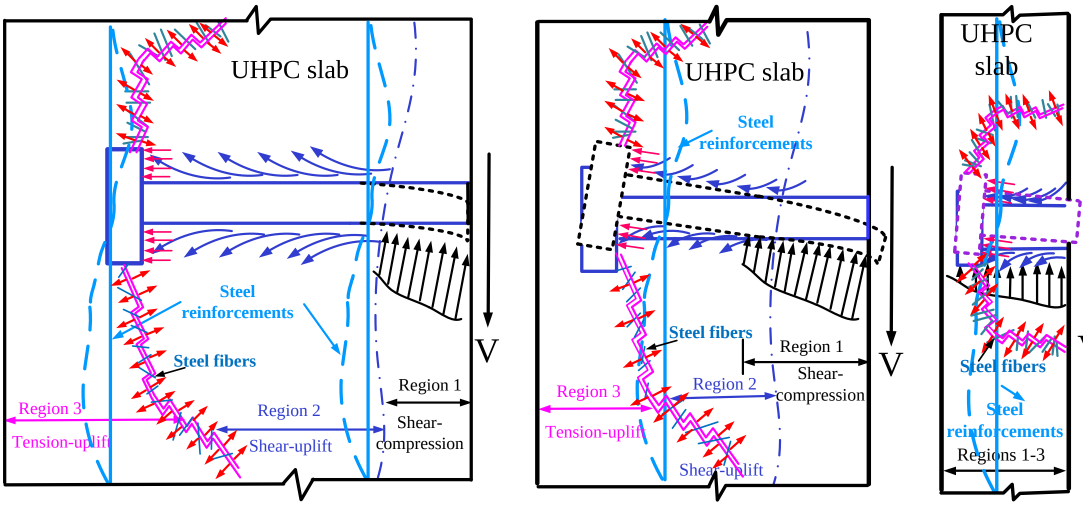

(a) D30T150 (b) D30T55 (c) D30T35

Fig. 9 Schematic of mechanisms of stud–UHPC interaction

Effects of stud aspect ratio

It was observed from Table 3 and Fig. 10 that the shear strength for specimens with 22 mm diameter studs experienced only an 8% variation as the aspect ratio decreased from 2.0 to 1.4, because stud fracture was a common failure mode across these specimens. The shear strength loss was marginal compared with that in the study by Kim et al. (2015)), where the stud aspect ratio was 4.5 and the diameter was 22 mm.

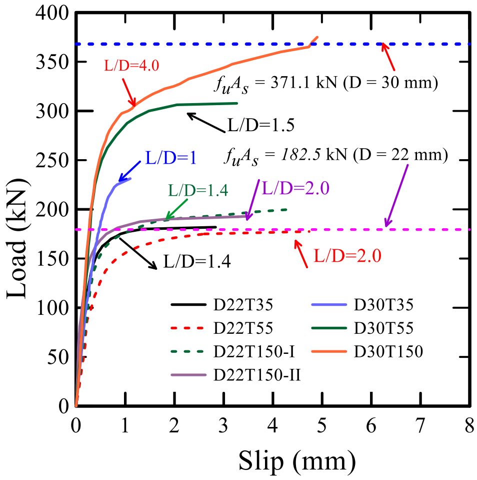

Fig. 10 Effects of stud aspect ratio

For 30 mm diameter studs the failure modes varied from stud complete / partial fracture to pullout as the aspect ratio decreased from 4.0 to 1.5 and 1.0. From complete to partial fracture the strength reduced by almost 25%, while from partial fracture to pullout failure the reduction was 35%. The peak slip tended to decrease with the aspect ratio reduction, because a smaller aspect ratio led to increased flexure of the stud. Note that the aspect ratios of D22T35 and D30T55 were similar, but failure modes and strengths differed.

The failure modes of pure shear, shear - tension and pure tension were all related to the stud aspect ratio. The ratio of predicted shear resistance to f_uA_s varied from 0.58 to 1.0, where f_u is the ultimate tensile strength and A_s is the cross-sectional area of the headed stud. A shear resistance due to stud failure in steel–NC composite structures can be safely predicted by f_uA_s if the stud aspect ratio exceeds 5.0 according to Pallarés and Hajjar (2010) or 4.2 according to Slutter and Driscoll (1961), Moreover, 0.8 f_uA_s is provided to predict the failure of studs with varying stud aspect ratios in Eurocode 4 (2 CEN 2005). According to the von Mises criterion, Pallarés and Hajjar (2010) recommended a ratio of 0.58 for pure shear failure of the stud and 0.65 for shear-dominated failure with a reliability index of approximately 4. Additionally, a ratio of 1.0 would be used to consider pure tension failure of the stud. In the current research, the shear strengths for large-diameter studs with aspect ratios of 1.5 and 1.0 were 19% and 40% lower, respectively, than that of the large stud with an aspect ratio of 4.0. Hence, the larger-diameter stud of aspect ratio 1.5 in UHPC showed great potential for obtaining 81% of its ultimate tensile strength at its fracture failure.

By contrast, UHPC pryout failure occurred at the lower aspect ratio of 1.0 for large-diameter studs. In the design codes of AISC 360 (American Institute of Steel Construction 2010) and Eurocode 4, the predicted concrete failure load is expressed by $A_s\sqrt{E_c f_c'}$, for which the coefficients are regulated as 0.37 and 0.5, respectively. In the present study, the coefficient for large-diameter studs with an aspect ratio of 1.0 corresponding to UHPC pry-out failure was suggested 0.13 based on the measured elastic modulus of the adopted UHPC, and needs further study to extrapolate given the limited number of specimens.

Regression analysis of connection behaviour

The shear strength, initial slip stiffness and ductility per stud for all specimens tested in this study are listed in Table 3, where both the average (Avg) value and the coefficient of variation (CoV) are given. The initial slip stiffness was calculated as the gradient of the straight line joining the points on the shear force vs slip curve at 10% and 40% of the ultimate load (Kim et al. 2015). The ductility refers to the ability to maintain a near-constant ultimate load across a wide range of slips, and hence it is here defined as the range of slip across which the load remained within 10% of the ultimate load.

Shear strength, initial slip stiffness and ductility comparisons are plotted in Fig. 11. It is seen that the average shear strength and initial slip stiffness increased as the stud diameter, aspect ratio and cover thickness increased. Note also that the ductility increased as the stud aspect ratio increased for a given stud diameter. It is interesting to observe that regular studs with an aspect ratio of 2 reached a highest ductility of 3.85 mm, and the ductility maybe reduced owing to the more pronounced flexure brought on by increasing aspect ratio. The ductility of 0.63 mm was obtained for large-diameter studs with an aspect ratio of 1.0, due to UHPC pryout failure significantly preceding plasticity of the stud.

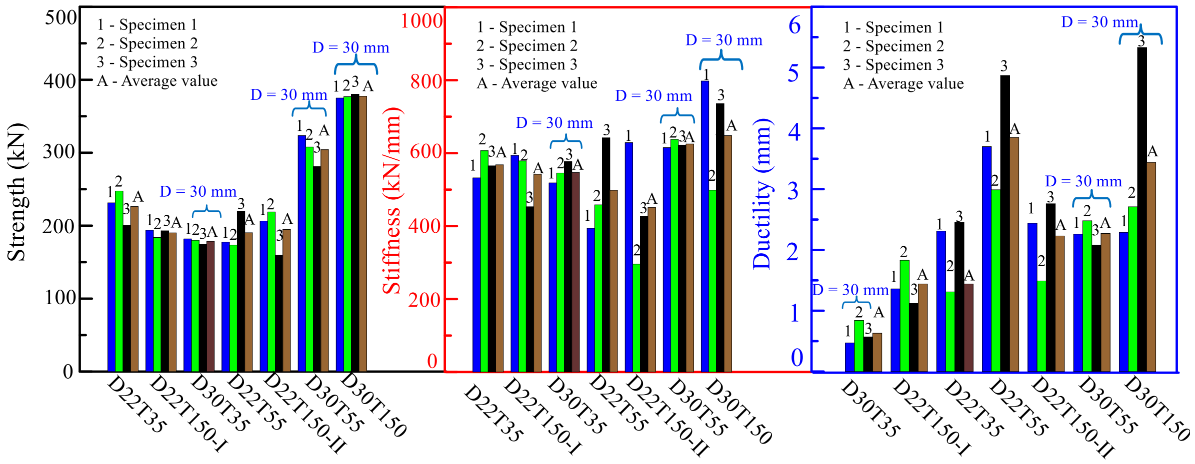

Fig. 11 Shear strength, stiffness and ductility of specimens

Based on the test results in this research, the shear strength, slip stiffness and ductility are plotted in normalized forms in Figs. (12-14). Fig.12 shows that the ratio of shear strength to ultimate tensile strength increased with increasing cover thickness and aspect ratio, and then stabilises when the stud aspect ratio and cover thickness exceed 2.0 and 50 mm respectively. The ratio of the shear stiffness to the cross-sectional area (Fig.13) firstly tended to increase and then decrease with the larger aspect ratio and cover thickness. Additionally, Fig.14 shows that the ductility ratio Δ_u / d_s (quotient of slip displacement ductility to stud diameter) increased with aspect ratio and then almost kept stable. For the influence of cover thickness, the ratio Δ_u / d_s seemed to first decrease and then increase. Also observe that ductility decreased with the increased stud diameter at thin cover, but increased with larger diameter stud at a thicker cover. These findings provide the references to the application of ultra-short stud-thin UHPC slab connections.

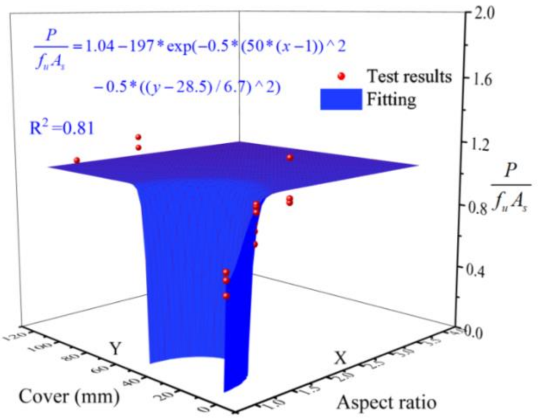

Fig. 12 Shear strengths variations with cover and stud aspect ratio

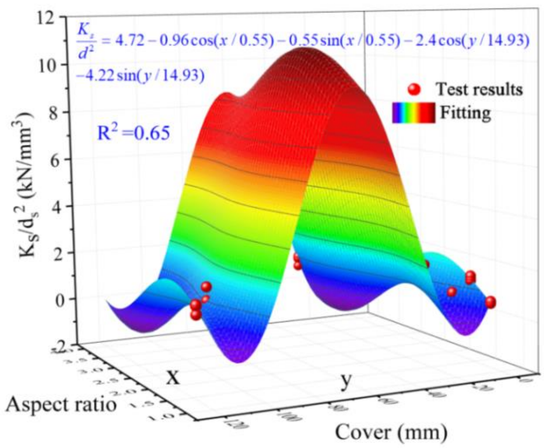

Fig. 13 Initial slip stiffness variations with cover and stud aspect ratio

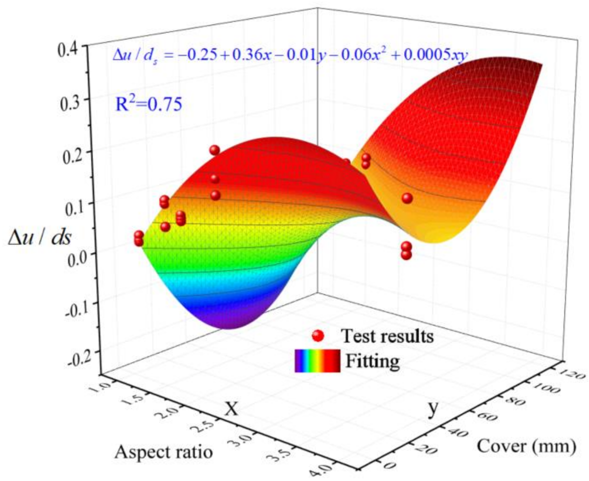

Fig. 14 Ductility variations with cover and stud aspect ratio

Directly related the plots of Figs 12-14, the shear strength, initial slip stiffness and ductility are now shown by regression analysis based on the experimental data to satisfy Eqs. (1 - 3) written below as functions of stud diameter, stud aspect ratio and cover thickness.

$$P_u = f_u A_s \{1.04 - 197 \exp[-\frac{1}{2}(50(\alpha - 1)^2 - \frac{1}{2}(\frac{c - 28.5}{6.7})^2]\} \quad \text{(Eq.1)}$$

$$K_s = (4.72 - 0.96\cos\frac{\alpha}{0.55} - 0.55\sin\frac{\alpha}{0.55} - 2.4\cos\frac{c}{14.93} - 4.22\sin\frac{c}{14.93})\ d^2 \quad \text{(Eq.2)}$$

$$\Delta_u = (-0.25 + 0.36\alpha - 0.01c - 0.06\alpha^2 + 0.0005c\alpha)d_s \quad \text{(Eq.3)}$$

$$(f_c = 125MPa,\ d = 22\ and\ 30\ mm,\ c = 5\text{-}120\ mm,\ 1.0 \le \alpha = h_s / d_s \le 4.0)$$

where f_u is the ultimate tensile strength of the stud, A_s is the cross-sectional area of the stud, h_s is the stud length, d_s is the stud diameter, c is the cover thickness over the stud head, Δ_u is the slip range, α is the stud aspect ratio.

The shear capacity is an exponential function while the initial slip stiffness and the ductility slip are a sinusoidal function and a polynomial function, respectively, of the aspect ratio, in which the stud diameter, the UHPC cover thickness and the stud aspect ratio ranged in 22-30 mm, 5-120 mm and 1.0 - 4.0, respectively while the compressive strength of UHPC was 125 MPa. The quality of regression was evaluated by the coefficients of determination (R^2). Figs (12 – 14) show that the shear strength (R^2 = 0.81) and ductility (R^2 = 0.75) curve fits are very good ($R^2 \geq 0.75$), while the initial slip stiffness curve fit is moderately good (R^2 = 0.65). This is an initial attempt at understanding the data. In future, with more test data it will be possible to populate these spaces further and progress to more reliable functions of greater R^2 values and the mechanical analysis on the connection behavior affected by multiple parameters will be performed (Zhang et al. 2017b).

Comparison with stud connectors in normal concrete

Stud connections in normal concrete (NC) from other studies (An and Cederwall 1996; K. Saari et al. 2004; Shim et al. 2004; Xue et al. 2008; Zhou 1984) are now used as references for the present ultra-short stud - UHPC connections. From previous work on the stud connections, the threshold between the shank fracture and concrete crushing failure lies at a concrete compressive strength of 30-40 MPa (Kim et al. 2015). Regular and large-diameter stud connections exhibited shear stiffnesses of 451-568 kN/mm and 547-648 kN/mm respectively, exceeding by up to 62% the 231-400 kN/mm range for 13-30 mm stud-NC connections (Kim et al. 2015; Shim et al. 2004).

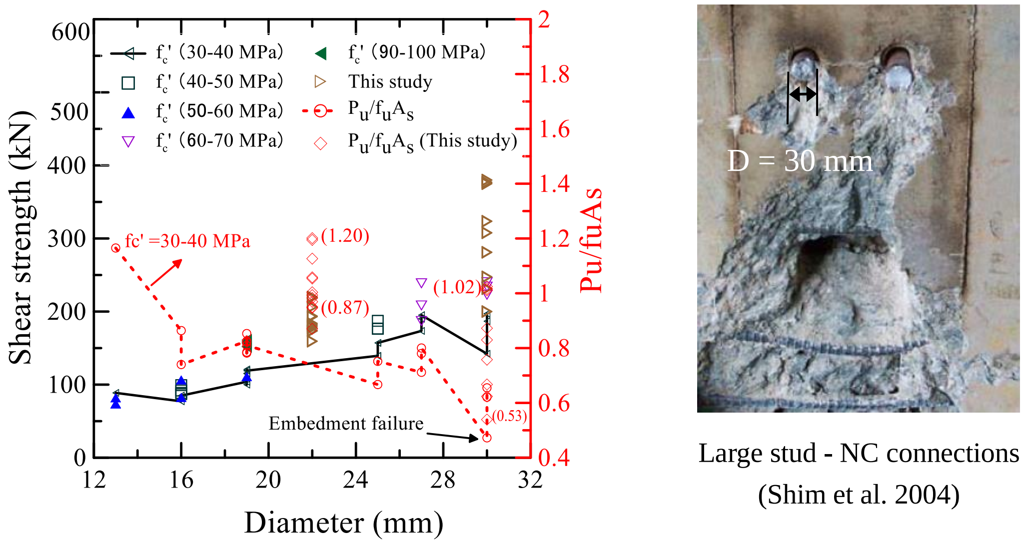

(a) Strength/Normalized strength- diameter relationships (b) Shank embedment failure

Fig. 15 Comparison of shear resistances for stud connections

Fig.15 shows the shear resistances of stud connections of different diameters and concrete strengths where the black line displays the shear resistances and the red line presents the force ratio (quotient between shear strength and stud ultimate tensile strength) for concretes of strength 30-40 MPa. Although shank failure always controls the shear strength for studs in UHPC, the aspect ratio also affected the shear resistance (Pallarés and

Hajjar 2010). For stud-NC connections, the force ratio (0.62-1.2 for stud fracture) largely decreases with increased stud diameter. Embedment failure (Fig. 15(b)) of 30mm diameter long stud-NC connections gave the lowest normalized shear strengths, achieving less than 50% of stud tensile resistance. Ultra-short studs in UHPC slabs showed improved force ratios of 0.82-1.2 for stud fracture and reached an average of 0.61 for UHPC pry-out failure.

Conclusions

Push-out tests were conducted to study the performance of ultra-short large diameter studs for application to lightweight steel–UHPC (ultra high performance concrete) composite bridges. The influences of stud diameter and aspect ratio, and cover concrete thickness over the stud head were included. The following conclusions are drawn:

(1) Connections with large (30 mm)-diameter studs of aspect ratio 2.0 - 1.5 failed by stud fracture, suggesting that stud strength might govern when short studs are used.

(2) At aspect ratios of 1.0 and 1.5, increasing the stud diameter changed the failure mode from complete or partial stud fracture with UHPC pryout, to only UHPC pryout. The UHPC failure modes of shear -compression, shear-uplift and tension-uplift potentially overlapped, thereby impairing the shear resistance of the involved UHPC. Thus, observed shear resistance increases of 26.7 % and 60% were not proportional to the increases in stud cross-sectional area, but were influenced by local crushing, cracking and UHPC pryout.

(3) Splitting cracks were observed in slabs with cover thickness not exceeding 30 mm. Cracks allowed pronounced flexure around the stud head and caused larger pryout force but lower shear force in the stud due to transverse expansion and reduced local triaxial stress.

(4) UHPC pryout failure may occur for short studs of aspect ratio 1.0, owing to insufficient anchorage. It is suggested to use $0.13A_s\sqrt{E_c f_c'}$ for the UHPC pryout resistance, while $f_u A_s$ is recommended to estimate the fracture failure load for short studs in thin UHPC slabs.

(5) Regression analysis shows that the longitudinal shear strength, initial slip stiffness and ductility of the stud-UHPC connections are exponential, sinusoidal and polynomial functions respectively of stud aspect ratio. Further test data will help clarify these functions.

(6) Relative to studs in normal concrete, ultra-short stud-UHPC connections show higher slip stiffnesses at lower aspect ratios and more closely approach the stud strengths.

(7) Given the bridge application, fatigue tests should also be conducted on the connections.

Data Availability Statement

All data, models, or codes that support the findings of this study are available from the corresponding author upon reasonable request.

Acknowledgment

This research was sponsored by the National Key R&D Plan (2017YFC07034), National Natural Science Foundation of China Youth Program (51908120), Natural Science Foundation of Jiangsu Province (BK 20180383), and Subote Materials Co. Ltd, Jiangsu, China. We would like to express our gratitude for their financial support to this research.

References

2 CEN. (2005). “Eurocode 4: Design of composite steel and concrete structures.” *Part 2: General rules for bridges*.

AASHTO. (2020). “AASHTO LRFD Bridge Design Specifications, 9th ed.” Washington, D.C.: American Association of State Highway and Transportation Officials.

An, L., and Cederwall, K. (1996). “Push-out tests on studs in high strength and normal strength concrete.” *Journal of Constructional Steel Research*, 36(1), 15–29.

ANSI/AISC (America National Standard Institute). (2010). “Specification for structural steel buildings.” *ANSI/AISC 360, Chicago*.

Cao, J., Shao, X., Deng, L., and Gan, Y. (2017). “Static and Fatigue Behavior of Short-Headed Studs Embedded in a Thin Ultrahigh-Performance Concrete Layer.” *Journal of Bridge Engineering*, American Society of Civil Engineers, 22(5), 04017005.

Cao, J., Shao, X., Zhang, Z., and Zhao, H. (2016). “Retrofit of an orthotropic steel deck with compact reinforced reactive powder concrete.” *Structure and Infrastructure Engineering*, Taylor & Francis, 12(3), 411–429.

GB 50010-2010. (2010). “Design Code for Concrete Structure.” China Planning Press, Beijing.

GB50017-2003, M. of construction of C. (2003). “Code for Design of Steel Structures.” *China Planning Press,Beijing*.

GB/T 31387-2015. (2015). *Reactive Powder Concrete*. National standards PR China.

Hamoda, A., Hossain, K. M. A., Sennah, K., Shoukry, M., and Mahmoud, Z. (2017). “Behaviour of composite high performance concrete slab on steel I-beams subjected to static hogging moment.” *Engineering Structures*, 140, 51–65.

Hossain, K. M. A., Alam, S., Anwar, M. S., and Julkarnine, K. M. Y. (2016). “High performance composite slabs with profiled steel deck and Engineered Cementitious Composite – Strength and shear bond characteristics.” *Construction and Building Materials*, 125, 227–240.

K. Saari, W., F. Hajjar, J., E. Schultz, A., and K. Shield, C. (2004). “Behavior of shear studs in steel frames with rein- forced concrete infill walls.” *Journal of Constructional Steel Research*, 60(10), 1453–1480.

Kim, J.-S., Kwark, J., Joh, C., Yoo, S.-W., and Lee, K.-C. (2015). “Headed stud shear connector for thin ultrahigh-performance concrete bridge deck.” *Journal of Constructional Steel Research*, 108, 23–30.

Kruszewski, D., Wille, K., and Zaghi, A. E. (2018). “Push-out behavior of headed shear studs welded on thin plates and embedded in UHPC.” *Engineering Structures*, 173, 429–441.

Lin, W., Yoda, T., Taniguchi, N., Kasano, H., and He, J. (2014). “Mechanical Performance of Steel-Concrete Composite Beams Subjected to a Hogging Moment.” *Journal of Structural Engineering*, American Society of Civil Engineers, 140(1), 04013031.

Lin, Z., Liu, Y., and Roeder, C. W. (2016). “Behavior of stud connections between concrete slabs and steel girders under transverse bending moment.” *Engineering Structures*, 117, 130–144.

Liu, T., Wang, Z., Guo, J., and Wang, J. (2019a). “Shear Strength of Dry Joints in Precast UHPC Segmental Bridges: Experimental and Theoretical Research.” *Journal of Bridge Engineering*, American Society of Civil Engineers, 24(1), 04018100.

Liu, Y., Zhang, Q., Bao, Y., and Bu, Y. (2019b). “Static and fatigue push-out tests of short headed shear studs embedded in Engineered Cementitious Composites (ECC).” *Engineering Structures*, 182, 29–38.

Liu, Y., Zhang, Q., Meng, W., Bao, Y., and Bu, Y. (2019c). “Transverse fatigue behaviour of steel-UHPC composite deck with large-size U-ribs.” *Engineering Structures*, 180, 388–399.

Luo, J., Shao, X., Fan, W., Cao, J., and Deng, S. (2019). “Flexural cracking behavior and crack width predictions of composite (steel + UHPC) lightweight deck system.” *Engineering Structures*, 194, 120–137.

Luo, Y., Hayashi Kazuhiro, and Nakashima Masayoshi. (2016a). “Behavior and Strength of Headed Stud–SFRCC Shear Connection. II: Strength Evaluation.” *Journal of Structural Engineering*, 142(2), 04015113.

Luo, Y., Hoki Kazuaki, Hayashi Kazuhiro, and Nakashima Masayoshi. (2016b). “Behavior and Strength of Headed Stud–SFRCC Shear Connection. I: Experimental Study.” *Journal of Structural Engineering*, 142(2), 04015112.

Meng, W., and Khayat, K. H. (2016). “Mechanical properties of ultra-high-performance concrete enhanced with graphite nanoplatelets and carbon nanofibers.” *Composites Part B: Engineering*, 107, 113–122.

Mosallam, A. S., Feo, L., Elsadek, A., Pul, S., and Penna, R. (2014). “Structural evaluation of axial and rotational flexibility and strength of web–flange junctions of open-web pultruded composites.” *Composites Part B: Engineering*, 66, 311–327.

Naaman, A. E., and Chandrangsu, K. (2004). “Innovative Bridge Deck System Using High-Performance Fiber-Reinforced Cement Composites.” *Structural Journal*, 101(1), 57–64.

Okada, J., Yoda, T., and Lebet, J.-P. (2006). “A study of the grouped arrangements of stud connectors on shear strength behavior.” *STRUCTURAL ENGINEERING / EARTHQUAKE*

ENGINEERING, 23(1), 75s–89s.

Ollgaard, J. G., Slutter, R. G., and Fisher, J. W. (1971). “Shear strength of stud connectors in lightweight and normal weight concrete, AISC Eng’g Jr., April 1971 (71-10).” 12.

Pallarés, L., and Hajjar, J. F. (2010). “Headed steel stud anchors in composite structures, Part I: Shear.” *Journal of Constructional Steel Research*, 66(2), 198–212.

Pavlović, M., Marković, Z., Veljković, M., and Buđevac, D. (2013). “Bolted shear connectors vs. headed studs behaviour in push-out tests.” *Journal of Constructional Steel Research*, 88, 134–149.

Precast/Prestressed Concrete Institute (PCI). (2004). *PCI design handbook: Precast and prestressed concrete. sixth edition Chicago (IL): Precast/Prestressed Concrete Insitute*.

Russell, H. G., and Graybeal, B. A. (2013). “Ultra-High Performance Concrete: A State-of-the-Art Report for the Bridge Community.”

Shafieifar, M., Farzad, M., and Azizinamini, A. (2018). “A comparison of existing analytical methods to predict the flexural capacity of Ultra High Performance Concrete (UHPC) beams.” *Construction and Building Materials*, (172), 10–18.

Shao, X., Qu, W., Cao, J., and Yao, Y. (2018). “Static and fatigue properties of the steel-UHPC lightweight composite bridge deck with large U ribs.” *Journal of Constructional Steel Research*, 148, 491–507.

Shao, X., Yi, D., Huang, Z., Zhao, H., Chen, B., and Liu, M. (2013). “Basic Performance of the Composite Deck System Composed of Orthotropic Steel Deck and Ultrathin RPC Layer.” *Journal of Bridge Engineering*, American Society of Civil Engineers, 18(5), 417–428.

Shim, C.-S., Lee, P.-G., and Yoon, T.-Y. (2004). “Static behavior of large stud shear connectors." *Engineering Structures*, 26(12), 1853–1860.

Slutter, R. G., and Driscoll, G. C. (1961). "Research on composite design at Lehigh University Research." *Chicago (IL): American Institute of Steel Construction*, 18–24.

Su, Q., Yang, G., and Bradford, M. A. (2014). "Static behaviour of multi-row stud shear connectors in high- strength concrete." *Steel and Composite Structures*, 17(6), 967–980.

Wang, J., Qi, J., Tong, T., Xu, Q., and Xiu, H. (2019a). "Static behavior of large stud shear connectors in steel-UHPC composite structures." *Engineering Structures*, 178, 534–542.

Wang, J., Xu, Q., Yao, Y., Qi, J., and Xiu, H. (2018). "Static behavior of grouped large headed stud-UHPC shear connectors in composite structures." *Composite Structures*, 206, 202–214.

Wang, J.-Y., Guo, J.-Y., Jia, L.-J., Chen, S.-M., and Dong, Y. (2017). "Push-out tests of demountable headed stud shear connectors in steel-UHPC composite structures." *Composite Structures*, 170, 69–79.

Wang, Z., Nie, X., Fan, J.-S., Lu, X.-Y., and Ding, R. (2019b). "Experimental and numerical investigation of the interfacial properties of non-steam-cured UHPC-steel composite beams." *Construction and Building Materials*, 195, 323–339.

Xue, D., Liu, Y., Yu, Z., and He, J. (2012). "Static behavior of multi-stud shear connectors for steel-concrete composite bridge." *Journal of Constructional Steel Research*, 74, 1–7.

Xue, W., Ding Min, Wang Hua, and Luo Ziwen. (2008). "Static Behavior and Theoretical Model of Stud Shear Connectors." *Journal of Bridge Engineering*, 13(6), 623–634.

Yang, I.-H., Joh, C., and Kim, B.-S. (2011). "Flexural strength of large-scale ultra high performance concrete prestressed T-beams." *Canadian Journal of Civil Engineering*, NRC

Research Press, 38(11), 1185–1195.

Yoo, S.-W., and Choo, J. F. (2016). “Evaluation of the flexural behavior of composite beam with inverted-T steel girder and steel fiber reinforced ultra high performance concrete slab.” *Engineering Structures*, 118, 1–15.

Yoshitake, I., Kuroda, Y., Watada, Y., and Kim, Y. J. (2016). “Fatigue performance of steel–concrete composite slabs with a cementitious adhesive subjected to water leakage.” *Construction and Building Materials*, 111, 22–29.

Zhang, Q., Liu, Y., Bao, Y., Jia, D., Bu, Y., and Li, Q. (2017a). “Fatigue performance of orthotropic steel-concrete composite deck with large-size longitudinal U-shaped ribs.” *Engineering Structures*, 150, 864–874.

Zhang, Q., Pei, S., Cheng, Z., Bao, Y., and Li, Q. (2017b). “Theoretical and Experimental Studies of the Internal Force Transfer Mechanism of Perfobond Rib Shear Connector Group.” *Journal of Bridge Engineering*, American Society of Civil Engineers, 22(2), 04016112.

Zhao, C., Wang, K., Zhou, Q., Deng, K., and Cui, B. (2018). “Full-Scale Test and Simulation on Flexural Behavior of Dovetail-Shaped Reactive Powder–Concrete Wet Joint in a Composite Deck System.” *Journal of Bridge Engineering*, American Society of Civil Engineers, 23(8), 04018051.

Zhou, S. (1984). “Strength and behavior of stud shear connectors for steel-concrete composite beams.” Thesis, Zhengzhou Institute of Technology, Zhengzhou,China,.

Zhu, Z., Yuan, T., Xiang, Z., Huang, Y., Zhou, Y. E., and Shao, X. (2018). “Behavior and Fatigue Performance of Details in an Orthotropic Steel Bridge with UHPC-Deck Plate Composite System under In-Service Traffic Flows.” *Journal of Bridge Engineering*, American Society of Civil Engineers, 23(3), 04017142.